
Letter

First detection of PSR B1259–63/LS 2883 in the Millimeter and Submillimeter Wavelengths with ALMA

Yutaka FUJITA^{1*}, Akiko KAWACHI², Takuya AKAHORI³, Hiroshi NAGAI³ and Masaki YAMAGUCHI⁴

¹Department of Earth and Space Science, Graduate School of Science, Osaka University, Toyonaka, Osaka 560-0043, Japan

²Department of Physics, School of Science, Tokai University, Kitakaname, Hiratsuka, Kanagawa 259-1292, Japan

³National Astronomical Observatory of Japan, 2-21-1 Osawa, Mitaka, Tokyo 181-8588, Japan

⁴Department of Physics, Faculty of Science and Engineering, Konan University 8-9-1 Okamoto, Kobe, Hyogo 658-8501, Japan

*E-mail: fujita@astro-osaka.jp

Received ; Accepted

Abstract

We report Atacama Large Millimeter/submillimeter Array (ALMA) observations of the binary system containing the pulsar PSR B1259–63 orbiting around a Be star LS 2883 after the 2017 periastron passage. We detected radio continuum emission from the binary system in the millimeter/submillimeter wavelengths for the first time. At Band 3 (97 GHz), the flux 84 days after the periastron is almost the same as that 71 days after the periastron. Although the binary system showed intense GeV gamma-ray flares during our observations, the Band 3 flux did not indicate any time correlation with them. The Band 3 fluxes are consistent with an extrapolation of the radio spectrum at lower frequencies. Assuming that it is synchrotron emission, we constrain magnetic fields ($\lesssim 0.6$ G) and the high-energy cutoff of the electrons ($\gamma \gtrsim 360$). The flux at Band 7 (343 GHz) 69 days after the periastron shows a significant excess from the extrapolation of the radio spectrum at lower frequencies. The flux may be associated with the circumstellar disk around the Be star. We also present the results of Australian Telescope Compact Array (ATCA) observations at 94 GHz for the 2014 periastron passage, which show that the radio spectrum was relatively soft when the pulsar passed the disk.

Key words: pulsars: individual: PSR B1259-63 — binaries: general — radio continuum: stars

1 Introduction

PSR B1259–63 is a 48 ms period rotation-powered pulsar in a highly eccentric ($e = 0.87$), 3.4 year orbit with a Be star LS 2883 (Johnston et al. 1992). The distance to the

binary is inferred to be 2.6 kpc (Miller-Jones et al. 2018). Be stars are known to have anisotropic stellar winds and an equatorial disk with enhanced mass outflow. Pulsar-timing data indicates that the circumstellar disk is inclined to the plane of the binary orbit (Melatos, Johnston, & Melrose

1995). The pulsar’s orbital radius at periastron is $\sim 21 R_*$, where $R_* \sim 9.2 R_\odot$ is the radius of the Be star LS 2883 (Negueruela et al. 2011). Because of the highly elliptical orbit, PSR B1259–63 is expected to interact with the equatorial disk of the Be star near the periastron (Okazaki et al. 2011; Takata et al. 2012).

The binary has been observed in multi-wavelengths. A double peaked non-thermal and unpulsed radio outburst takes place around a periastron passage, each of which reflects the disk crossing of the pulsar (Connors et al. 2002; Johnston et al. 2005). The radio emission seems to be synchrotron emission from electrons accelerated at the shock produced through the interaction between the pulsar wind and the disk or the stellar outflow. X-ray light curves also show the double-peak structure; this emission may be synchrotron emission or inverse Compton (IC) scattering (Chernyakova et al. 2006; Chernyakova et al. 2009; Uchiyama et al. 2009; Pétri & Dubus 2011; Chernyakova et al. 2015).

Unpulsed TeV gamma-ray emission has been detected with High Energy Stereoscopic System (HESS) close to the periastron passage (Aharonian et al. 2005; Aharonian et al. 2009). If the emission is IC scattering, the intense photon fields provided by the companion star and the disk serve as a target for the production of the high energy gamma-rays (Tavani et al. 1996; Kirk et al. 1999; Kong et al. 2011), although hadronic mechanisms may be possible (Kawachi et al. 2004; Neronov & Chernyakova 2007). In the GeV band, flares have been observed with the *Fermi Gamma-ray Space Telescope* after the periastron passage and after the passage of the dense equatorial disk of the Be star (Abdo et al. 2011; Caliendo et al. 2015; Tam et al. 2018; Johnson et al. 2018). The flares are apparently triggered by the disruption of the circumstellar disk (Chernyakova et al. 2015).

Despite these multi-wavelength observations, there are yet-to-be explored bands. While previous radio observations have been limited to the frequencies of $\nu \lesssim 10$ GHz, no information has been obtained at $\nu \gtrsim 10$ GHz. Observations in this band could elucidate a link between the radio and X-ray emissions. For example, if there is a cutoff in this band, the X-ray emission is likely to be produced by a mechanism that is different from that of the radio emission. In that case, IC scattering is a likely solution (Chernyakova et al. 2006). If not, the X-ray emission could be synchrotron emission, which is the same as the radio emission, although it is not conclusive. Moreover, the emission from the circumstellar disk around the Be star could be observed in this band. It is important to reveal this emission because the radiation field can affect the gamma-ray emission from the binary through IC scattering

(van Soelen, & Meintjes 2011; van Soelen et al. 2012).

In this letter, we report the detection of the binary system PSR B1259–63 at 97 and 343 GHz after the 2017 periastron passage with Atacama Large Millimeter/submillimeter Array (ALMA) for the first time. We also present Australian Telescope Compact Array (ATCA) observations at 94 GHz for the 2014 periastron passage.

2 Observations

2.1 ALMA

ALMA Band 3 ($\lambda = 3$ mm) observations were carried out on 2017 December 2 with forty-two 12 m antennas and December 15 with forty-five 12 m antennas, and Band 7 ($\lambda = 0.9$ mm) observation was carried out on 2017 November 30 with forty-seven 12 m antennas (project code: 2017.1.01188.S). The data were taken with time division mode (TDM) centered at 97 GHz for Band 3 and 343 GHz for Band 7. The total on-source time is about 5 minutes for all three observations. The data were processed with the CASA/ALMA Pipeline (Pipeline-CASA51-P2B) in a standard manner. Bandpass characteristics were corrected in both amplitude and phase using bandpass calibrator J1647-5848 and J1337-1257 in Band 3 and Band 7, respectively. Gain calibration was done using phase calibrator J1322-6352 and J1308-6707 in Band 3 and Band 7, respectively, with the aid of phase correction with the water vapor radiometer. Amplitude scaling was derived with the bandpass calibrator.

Images were created by combining all spectral windows in each band. Deconvolution was done using the CASA task `tclean` with the Briggs weight of robust parameter of 0.5. Table 1 summarizes the image rms and angular resolution. We refer to the periastron passage time as t_p regardless of periastron passages. We detected a compact, single component in both Band 3 and 7. The flux was evaluated as the total flux density derived by a Gaussian model fitting.

We note that the ALMA fluxes include the pulsed component of the pulsar. However, the observations at lower frequencies (\sim a few GHz) show that the flux of the pulsed component is a few mJy and the component has a spectrum approximately given by $\propto \nu^{-1}$ (Johnston et al. 2005). Thus, it can safely be ignored at the ALMA bands.

2.2 ATCA

The observations at 3 mm wavelength (94 GHz) with ATCA were also carried out around and after the 2014 periastron passage of the binary. The ATCA consists of six

Table 1. Angular resolution, image rms, and observed fluxes for the ALMA observations in 2017

Band	Date	Day (from t_p)	Beam Shape	Image RMS ($\mu\text{Jy beam}^{-1}$)	Observed Flux (mJy)
3 (97 GHz)	Dec 2	+71	$0.35'' \times 0.21''$ at 78°	41	1.1 ± 0.1
3 (97 GHz)	Dec 15	+84	$0.42'' \times 0.36''$ at -52°	36	0.97 ± 0.09
7 (343 GHz)	Nov 30	+69	$0.056'' \times 0.043''$ at -8°	87	2.3 ± 0.4

Table 2. The calibrators and observed fluxes for the ATCA observations in 2014

Date	Day (from t_p)	Observing Time (min)	Calibrators			Residual RMS (1σ) (mJy)
			Bandpass	Flux	Gain/Phase	
Apr 4	-29.9	20	PKS 1253-055	Mars	PKS 1305-668	3.58
Apr 6	-27.8	286	PKS 0537-441	Jupiter	PKS 1305-668	0.853
May 19	+15.4	82	PKS 1921-293	Uranus	PKS 1305-668	1.550
May 27	+23.3	68	PKS 1253-055	Uranus	PMN J1326-5256	0.704
Jun 15	+42.2	74	PKS 1921-293	Saturn	PMN J1326-5256	0.466
Jun 29	+56.1	71	PKS 1253-055	Mars	PMN J1326-5256	0.139
Sep 26	+145.6	58	PKS 0537-441	Jupiter	PMN J1326-5256	1.43

22 m radio antennas of which five are available for 3 mm observations. The Compact Array Broadband Backend (CABB) provides observations with two 2048 MHz intermediate frequencies (IF) bands which are centered at 93.504 GHz and 95.552 GHz. The target was observed with several sets of 10 minute on-source observations in between the observations of the gain/phase calibrator. The calibrators for the bandpass, flux density and gain/phase of each observation are summarized in Table 2. The pulsar-binning mode was not employed in the observations based on the similar pulse flux estimation in the previous ALMA section. The data was processed using the data reduction package MIRIAD (Sault, Tueben & Wright 1995). A Gaussian fit was performed on the Stokes I images with the MIRIAD task `imfit`, and when no detection was confirmed, the residual rms error over the image (table 2) is used to obtain the upper limit (figure 2). The inverted images are produced to minimize the noise level for better sensitivity.

3 Results and Discussion

The most recent periastron passage of the PSR B1259-63/LS 2883 system occurred on MJD 58018.143 (UTC 2017 September 22 03:25:55.2). In table 1 and figure 1, we show the radio fluxes of PSR B1259-63 obtained with ALMA. At 97 GHz, we observed the object twice ($t_p + 71$ and $t_p + 84$ days) and found that their fluxes are identical within the errors. For a comparison, we show unpulsed (total minus pulsed) radio fluxes at 1384, 2496, 4800, and 8400 MHz obtained with ATCA at similar post-periastron days at the 2000 and 2004 periastron passages. Unfortunately, observational results for the 2007-2017 periastron passages at those low frequencies have not been

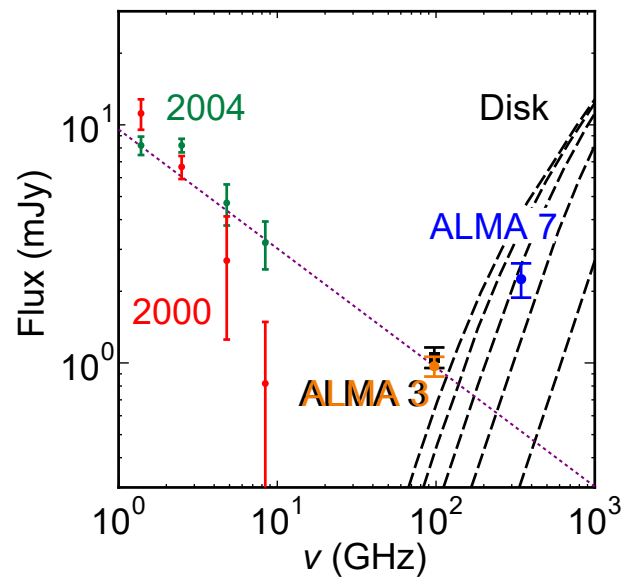


Fig. 1. Radio fluxes of PSR B1259-63. Those obtained with ALMA are shown by the filled black square (Band 3 or 97 GHz at $t_p + 71$ days), the filled orange circle (Band 3 at $t_p + 84$ days), and the filled blue circle (Band 7 or 343 GHz at $t_p + 69$ days). Unpulsed fluxes obtained with ATCA at $t_p + 63.4$ days at the 2000 passage are shown by red dots (Connors et al. 2002) and those at $t_p + 64.2$ days at the 2004 passage are shown by green dots (Johnston et al. 2005). The dotted purple line is a spectrum represented by $S_\nu \propto \nu^{-0.5}$. The normalization is set so that the line passes the second ALMA Band 3 observation (filled orange circle). Dashed black lines show the infrared emission from the Be star's circumstellar disk for different disk sizes predicted by van Soelen, & Meintjes (2011). The disk sizes are (from the bottom to the top) 10, 20, 30, 40 and 50 R_* .

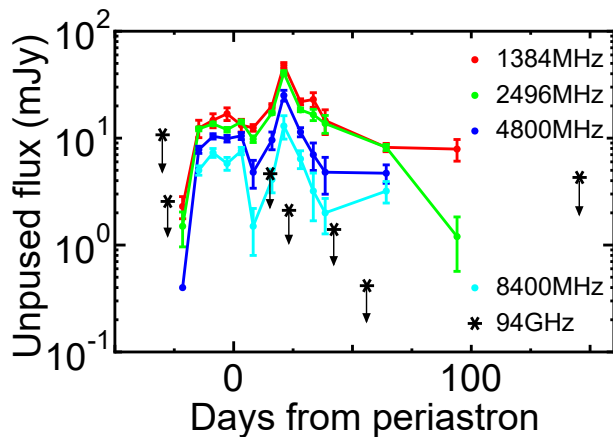


Fig. 2. ATCA upper limits (3σ) at 94 GHz for the 2014 periastron passage are shown by stars. Lines are light curves of the unpulsed emission for the 2004 periastron passages (Johnston et al. 2005). Each line displays four different frequencies, 1384, 2496, 4800 and 8640 MHz, in order from top down.

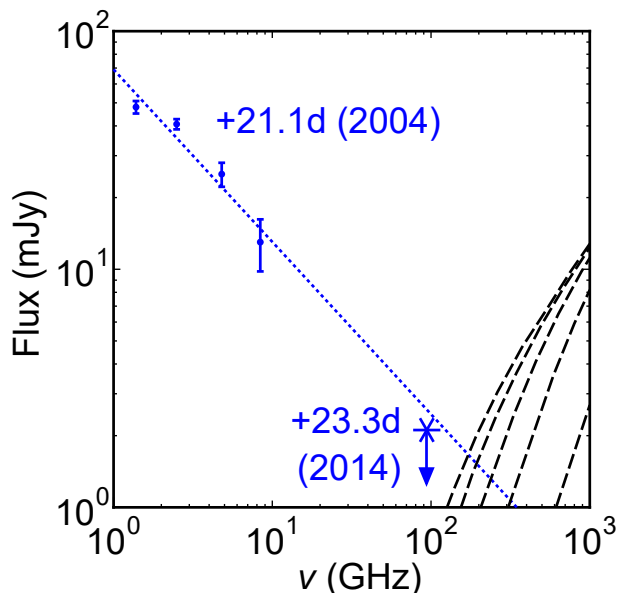


Fig. 3. Stars are ATCA upper limits (3σ) at 94 GHz for the 2014 periastron passage at $t_p + 23.3$ days. Dots are fluxes for the 2004 periastron passage at $t_p + 21.1$ days (Johnston et al. 2005). Dotted line is a power-law fit for the data for the 2004 periastron passage ($\propto \nu^{-0.72}$). Dashed black lines show the infrared emission from the Be star's circumstellar disk, and they are the same as those in figure 2.

published. However, Johnston et al. (2005) indicated that the light curve of the unpulsed radio emission at 1384 MHz is broadly similar from one periastron to the next. The spectrum at the 2000 periastron passage is steeper than that at the 2004 periastron passage (figure 1). While for the former the fluxes at 4.8 and 8.4 GHz may be affected by phase-calibration errors (Connors et al. 2002), we cannot deny the possibility that the spectrum at those and higher frequencies is highly time dependent. The thin dotted purple line represents a spectrum of $S_\nu \propto \nu^{-0.5}$. It shows that the ALMA Band 3 fluxes can be regarded as an extrapolation of the ATCA fluxes for the 2004 periastron passage. The power-law spectrum with a negative index implies that the radio emission is a synchrotron emission.

PSR B1259–63 is known to become active after a periastron passage in the GeV gamma-ray band. For the 2017 periastron passage, the gamma-ray activities were more intense than the previous ones and displayed variability of short timescales (~ 1.5 minutes). These activities were observed from $\sim t_p + 40$ days to $\sim t_p + 75$ days (Tam et al. 2018; Johnson et al. 2018). Thus, while our first Band 3 observation ($t_p + 71$ days) was performed during the active period, the second observation ($t_p + 84$ days) was done outside the period. The stable radio flux between the two observations suggests that the origin of the radio synchrotron emission is different from that of the gamma-ray emission.

Figure 1 indicates that the flux at the ALMA Band 7 (343 GHz) at $t_p + 69$ days is clearly above the extrapolation from the fluxes at low frequencies (thin dotted purple line). This suggests that the flux is not attributed to the synchrotron emission. The most plausible explanation is that the emission comes from the circumstellar disk around the Be star, which supplies seed photons for gamma-ray production through IC scattering (Khangulyan et al. 2012; van Soelen et al. 2012). The dashed black lines in figure 1 show a prediction of the disk emission (van Soelen, & Meintjes 2011). The Band 7 flux is consistent with the spectrum when the disk radius is $\sim 30 R_*$. This radius is smaller than the one simply expected from pulsar eclipses ($\sim 50 R_*$; van Soelen, & Meintjes 2011). The discrepancy may be caused by disruption of the disk by the pulsar passage or by model uncertainties. In order to discriminate the two possibilities, it would be useful to observe the object at different times before and after the disk passage and see if the flux of the possible disk component changes.

The Band 3 fluxes are above the predicted disk emission (figure 1), which also suggests that they are synchrotron emission. The extension of the synchrotron emission up to 97 GHz constrains the magnetic fields of the system (B) if electrons are instantaneously injected. Since the spectrum is presented by a power-law, electrons that ra-

diate the emissions at $\lesssim 97$ GHz are not affected by synchrotron loss until at least $\sim t_p + 84$ days. Assuming that synchrotron emission at the frequency of ν is produced by electrons with a Lorentz factor of γ , the relation between ν and γ is

$$\nu \sim 0.29 \nu_c \equiv 0.29 \frac{3\gamma^2 e B \sin \alpha}{4\pi m_e c}, \quad (1)$$

where e is the unit charge, α is the pitch angle of the electrons, m_e is the electron mass, and c is the light speed (Rybicki & Lightman 1979). If electrons with a power-law spectrum are instantaneously injected at $t = 0$, and if they passively evolve being affected by synchrotron loss, the electrons with Lorentz factors larger than γ will have been removed at $t = T$, where

$$\gamma = \frac{1}{b_1 T} \quad (2)$$

(Sarazin 1999). The factor b_1 is related to the synchrotron loss rate for $\gamma \gg 1$:

$$-\frac{d\gamma}{dt} = \frac{4}{3} \frac{\sigma_T}{m_e c} \frac{B^2}{8\pi} \gamma^2 \equiv b_1 \gamma^2 \quad (3)$$

(Sarazin 1999). By eliminating γ from equations (1) and (2), the magnetic field is written as

$$B = 0.6 (\sin \alpha)^{1/3} \left(\frac{\nu}{97 \text{ GHz}} \right)^{-1/3} \left(\frac{T}{64 \text{ days}} \right)^{-2/3} \text{ G}. \quad (4)$$

Here, we assumed that the electrons were injected when the pulsar passed through the disk around the Be star at $\sim t_p + 20$ days (Johnston et al. 2005). If the electrons are affected by adiabatic cooling and the magnetic-field strength is a decreasing function of time (Tavani, & Arons 1997; Connors et al. 2002), the field at the observation ($\sim t_p + 84$ days) must be weaker. Thus, equation (4) shows that the magnetic field associated with the synchrotron emission is $B \lesssim 0.6$ G. This field strength is roughly consistent with the predicted ones around the shock created through the interaction of the pulsar wind with the outflow from the Be star (Tavani, & Arons 1997; Ball et al. 1999), and the values deduced from the observed radio, X-ray and gamma-ray emissions near the periastron (Connors et al. 2002; Aharonian et al. 2005). If we assume that $B = 0.6$ G and $T = 64$ days, the Lorentz factor is $\gamma = 360$ [equation (2)]. Thus, the cooling cutoff in the electron energy spectrum should be at $\gamma > 360$. If the spectrum further extends to higher energies, the X-ray emission of the binary can also be explained by the synchrotron emission.

For the 2014 periastron, which happened on 2014 May 4 ($t_p = \text{MJD } 56781.42$), we obtained only image rms (1σ) at 94 GHz with ATCA (table 2), from which we estimate 3σ upper limits of the flux (figure 2). For comparison, we present light curves for the 2004 periastron passage; they have a peak at $\sim t_p + 20$ days, which corresponds to the

disk passage of the pulsar (Johnston et al. 2005). Figure 3 shows the radio spectrum at the disk passage. The upper limit at 94 GHz is below the extrapolation of lower frequency fluxes ($\propto \nu^{-0.72}$). This means that the spectrum is relatively soft and is not hardened during the passage. The relatively small flux at 94 GHz could constrain theoretical models of particle acceleration through interaction between the pulsar wind and the disk. For example, the acceleration would take some time to form a power-law spectrum up to the high frequency.

4 Conclusion

We have reported the results of ALMA observations of the pulsar-Be star binary PSR B1259–63/LS 2883 at 97 and 343 GHz after the 2017 periastron passage. We detected the object at both frequencies for the first time. We found that the flux at 97 GHz does not change between our two observations (interval of 13 days) and it does not have a time correlation with intense gamma-ray flares. The flux is consistent with an extrapolation of the spectrum at lower frequencies of $\lesssim 10$ GHz, which means that the radio synchrotron emission extends at least up to 97 GHz. Assuming that the electrons that are responsible for the synchrotron emission are injected when the pulsar passes through the circumstellar disk of the companion star, the magnetic-field strength and the cooling-cutoff energy of the electrons can be constrained to be $B \lesssim 0.6$ G and $\gamma \gtrsim 360$, respectively. The flux at 343 GHz is much larger than the extrapolation of the low-frequency observations. This may indicate that the emission comes from the circumstellar disk of the Be star. We have also presented ATCA observations at 94 GHz for the 2014 periastron passage. They showed that the radio spectrum is not hardened during the disk passage of the pulsar. Our results could be new information that constrains theoretical models.

Acknowledgments

This work was supported by MEXT KAKENHI No. 18K03647 (Y.F.) and JP18K03709 (H.N.). M.Y. was supported by Hayakawa Fund. We acknowledge Dr. Jamie Stevens, CSIRO's Senior Systems Scientist at the Australian Telescope Compact Array for his support. This paper makes use of the following ALMA data: ADS/JAO.ALMA#2017.1.01188.S. ALMA is a partnership of ESO (representing its member states), NSF (USA) and NINS (Japan), together with NRC (Canada), MOST and ASIAA (Taiwan), and KASI (Republic of Korea), in cooperation with the Republic of Chile. The Joint ALMA Observatory is operated by ESO, AUI/NRAO and NAOJ.

References

- Abdo, A. A., Ackermann, M., Ajello, M., et al. 2011, *ApJ*, 736, L11
- Aharonian, F., Akhperjanian, A. G., Aye, K.-M., et al. 2005, *A&A*, 442, 1
- Aharonian, F., Akhperjanian, A. G., Anton, G., et al. 2009, *A&A*, 507, 389
- Ball, L., Melatos, A., Johnston, S., & Skjæ Raasen, O. 1999, *ApJL*, 514, L39
- Caliandro, G. A., Cheung, C. C., Li, J., et al. 2015, *ApJ*, 811, 68
- Chernyakova, M., Neronov, A., Aharonian, F., Uchiyama, Y., & Takahashi, T. 2009, *MNRAS*, 397, 2123
- Chernyakova, M., Neronov, A., Lutovinov, A., Rodriguez, J., & Johnston, S. 2006, *MNRAS*, 367, 1201
- Chernyakova, M., Neronov, A., van Soelen, B., et al. 2015, *MNRAS*, 454, 1358.
- Connors, T. W., Johnston, S., Manchester, R. N., & McConnell, D. 2002, *MNRAS*, 336, 1201
- Johnston, S., Ball, L., Wang, N., et al. 2005, *MNRAS*, 358, 1069
- Johnston, S., Manchester, R. N., Lyne, A. G., et al. 1992, *ApJL*, 387, L37
- Johnson, T. J., Wood, K. S., Kerr, M., et al. 2018, *ApJ*, 863, 27
- Kawachi, A., Naito, T., Patterson, J. R., et al. 2004, *ApJ*, 607, 949
- Khangulyan, D., Aharonian, F. A., Bogovalov, S. V., et al. 2012, *ApJ*, 752, L17.
- Kirk, J. G., Ball, L., & Skjæraasen, O. 1999, *Astroparticle Physics*, 10, 31
- Kong, S. W., Yu, Y. W., Huang, Y. F., & Cheng, K. S. 2011, *MNRAS*, 416, 1067
- Melatos, A., Johnston, S., & Melrose, D.B. 1995, *MNRAS*275, 381
- Miller-Jones J.C.A. et al., 2018, *MNRAS*479, 4849
- Negueruela, I., Ribó, M., Herrero, A., Lorenzo, J., Khangulyan, D., & Aharonian, F.A., 2011, *ApJ*, 732, L1
- Neronov, A., & Chernyakova, M. 2007, *Ap&SS*, 309, 253
- Okazaki, A. T., Nagataki, S., Naito, T., et al. 2011, *PASJ*, 63, 893
- Pétri, J., & Dubus, G. 2011, *MNRAS*, 417, 532
- Rybicki, G. B., & Lightman, A. P. 1979, *Radiative Processes in Astrophysics* (New York: John Wiley & Sons)
- Sarazin, C. L. 1999, *ApJ*, 520, 529
- Sault, R. J., Teuben, P. J., & Wright, M. C. H. 1995, in *Astronomical Data Analysis Software and Systems IV*, *Astronomical Society of the Pacific Conference Series*, Vol. 77, R. A. Shaw, H. E. Payne & J. J. E. Hayes eds., 433
- Takata, J., Okazaki, A. T., Nagataki, S., et al. 2012, *ApJ*, 750, 70.
- Tam, P. H. T., He, X.-B., Pal, P. S., et al. 2018, *ApJ*, 862, 165
- Tavani, M., & Arons, J. 1997, *ApJ*, 477, 439
- Tavani, M., Grove, J. E., Purcell, W., et al. 1996, *A&AS*, 120, 221
- Uchiyama, Y., Tanaka, T., Takahashi, T., et al. 2009, *ApJ*, 698, 911
- van Soelen, B., & Meintjes, P. J. 2011, *MNRAS*, 412, 1721
- van Soelen, B., Meintjes, P. J., Odendaal, A., et al. 2012, *MNRAS*, 426, 3135